41st AIAA/ASME/SAE/ASEE Joint Propulsion Conference and Exhibit
10-13 July 2005, Tucson, Arizona
AIAA-2005-4402

Internal Plasma Structure Measurements of a Hall Thruster Using Plasma Lens Focusing

Jesse A. Linnell* and Alec D. Gallimore†
Plasmadynamics and Electric Propulsion Laboratory, Department of Aerospace Engineering, University of Michigan Ann Arbor, MI 48109 USA

Magnetic field topology has been found to be a central design concern for high-efficiency Hall thrusters. For future improvements in Hall thruster design, it is necessary to better understand the effects that magnetic field topology has on the internal plasma structure. The Plasmadynamics and Electric Propulsion Laboratory's High-speed Axial Reciprocating Probe system using a floating emissive probe is used to map the internal structure of the NASA-173Mv1 Hall thruster. Measurements are taken at 300 and 500 V operating with xenon at 102.4 sccm anode flow rate with and without the trim coil operating. Electron temperature and electric field are also measured and reported. The acceleration zone and equipotential lines are found to be strongly linked to the magnetic field lines. Moreover, in some cases the ions are accelerated strongly toward the center of the discharge channel. These results have strong implications on the performance and lifetime optimization of Hall thrusters.

I. Introduction

Hall thrusters[1,2] are space propulsion devices that use crossed electric and magnetic fields to ionize and accelerate propellant atoms to high exhaust velocities. The electric field is established by an electron current that crosses and is concurrently impeded by the magnetic field. The magnetic field causes the electrons to follow a closed drift path and for this reason Hall thrusters are often referred to as closed drift thrusters. The magnetic field has been shown to have a strong effect on the overall Hall thruster efficiency.[3-5] The focus of this research is to study the effects that the magnetic field topology has on the internal plasma structure of Hall thrusters.

An important magnetic field topological feature in any state-of-the-art Hall thruster is what is commonly referred to as a plasma lens.[1,3,4,6-8] A plasma lens uses magnetic field lines that have a curvature that focus ions toward the center of the discharge channel. To first order, the magnetic field lines chart the equipotential lines inside a Hall thruster. Which explains the strong focusing effect that has been displayed with the NASA-173Mv1.[3,4] The NASA-173Mv1 Hall thruster utilizes a plasma lens topology that has been shown to improve beam focusing, ion acceleration processes and internal electron dynamics.[4,5]

This research employs a floating emissive probe that is swept at high speeds into the Hall thruster discharge channel to map the internal plasma structure. This high-speed motion reduces plasma perturbations and allows for accurate plasma potential measurements in the harsh thruster environment. Previous work has used similar methods to characterize the internal potential structure of Hall thrusters.[9-14] Haas[9] also mapped the entire discharge channel of the UM/AFRL P5 with this technique, which he pioneered. Only by mapping the entire discharge channel will it be possible to study the full effect of the magnetic field. Haas noticed strong defocusing equipotential lines in the P5 at a discharge voltage and current of 300 V and 10 A, respectively. Keidar[15] shows that this behavior is related to a change in the electron mobility due to the magnetic field gradient and due to a radial electron temperature gradient. The present work is unique in that the NASA-173Mv1 has a vastly different magnetic field topology and the potential structure is expected to be unlike the P5's.

* Ph.D Candidate, Aerospace Engineering, jlinnell@umich.edu, 1919 Green Rd Room B107, Member AIAA.
† Professor and Laboratory Director, Aerospace Engineering, alec.gallimore@umich.edu, Associate Fellow AIAA.

II. Experimental Apparatus

A. Facility

The measurements reported in this paper were conducted in the Large Vacuum Test Facility (LVTF) at the University of Michigan's Plasmadynamics and Electric Propulsion Laboratory (PEPL). The LVTF is a cylindrical stainless-steel tank, which is 9 m long and 6 m in diameter. The vacuum chamber is evacuated using seven CVI model TM-1200 internal cryopumps, which combined are capable of pumping 240,000 l/s of xenon. The vacuum tank pressure is monitored by using two hot-cathode ionization gauges. The vacuum chamber operates at a base pressure of 1.5×10^{-7} Torr and approximately 3.3×10^{-6} Torr (corrected[16]) during most thruster operating points.

High-purity research grade xenon is used as propellants for the following measurements. The purity level of xenon are 99.9995%. The propellant is supplied through the propellant feel lines using 20 and 200 sccm mass flow controllers for the cathode and anode, respectively. The mass flow controllers are calibrated using a constant volume method. The compressibility correction factor is calculated using the van der Waals Equation[17] and the Virial Equation.[18] Error in the mass flow controllers is approximately ±1% of full scale.

B. Thruster

The NASA-173Mv1 Hall thruster[4] (Fig. 1) is used for all measurements. In addition to the standard inner and outer magnetic coils, the NASA-173Mv1 uses a trim coil to create a highly adaptable magnetic field topology. As discussed earlier, the magnetic field created by the trim coil is found to improve thruster efficiency by establishing an electrostatic plasma lens. The thruster is run for one hour for the initial conditioning and is warmed up for at least 30 minutes at a given operation point before data are taken.

A Busek BHC-50-3UM hallow cathode is used for all measurements. The cathode flow rate is equal to 10% of the anode flow rate with a minimum of 0.93 sccm. The cathode axial centerline is mounted 30 degrees off horizontal and the center of the cathode orifice is placed 30 mm downstream and 30 mm above the thruster outer face.

Example magnetic fields for the NASA-173Mv1 are given in Fig. 2.[3] Figure 2 shows what is commonly referred to as the magnetic lens and the effect of the trim coil on increasing the concavity of the magnetic lens.

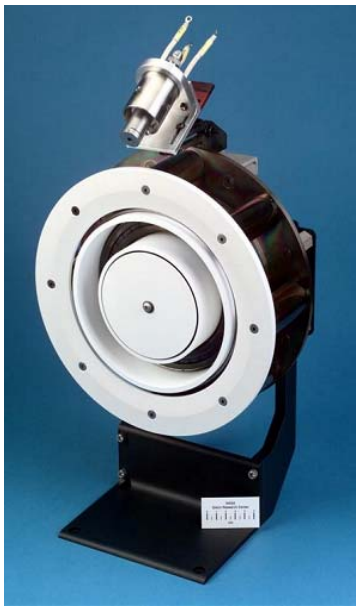

Figure 1. NASA-173Mv1 Hall Thruster

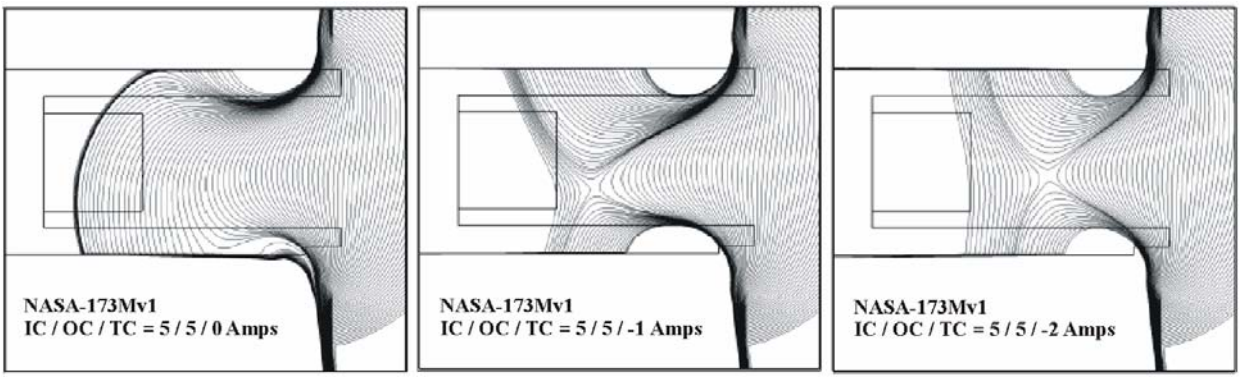

Figure 2. Example magnetic field topology of the NASA-173Mv1 at constant inner and outer magnet currents at several trim coil currents. (Ref. 3)

C. High-Speed Axial Reciprocating Probe

The High-Speed Axial Reciprocating Probe[19,20] (HARP) is a linear motor assembly providing direct linear motion at very high speed and large acceleration. The linear motor is an LM210 manufactured by Trilogy that has a three-phase brushless DC servomotor consisting of a linear, "U"-shaped magnetic track and a "T"-shaped coil moving on a set of linear tracks. A linear encoder provides positioning resolution to 5 microns. The table is covered by a stainless steel and graphite shroud to protect the HARP from excessive heating and high-energy ions. One side has a thin slit running the length of the table through which a probe boom extends.

D. Emissive Probe

The emissive probe design is based on a combination of the work done by PEPL[9] and Princeton Plasma Physics Laboratory (PPPL).[21] The emissive probe is composed of 1.5-mm-diameter double bore alumina insulator. The emitting filament is 1% thoriated tungsten with a diameter of 0.0127 cm. The electrical connection along the length of the probe is completed using 30 AWG copper leads that are slightly recessed into the alumina shaft. Additional short lengths of thoriated tungsten wire are inserted into the alumina tubing to provide a tight fit and guarantee good contact between the emitter and copper wires. Plasma perturbations are in part caused by the alumina probe releasing secondary electrons into the discharge channel. Efforts were made to use a low secondary electron emitting segmented coating[21] on alumina shaft to reduce plasma perturbations. A coating of 95% graphite paint is applied to the alumina in ringlets. The ringlets are approximately 1 mm in width with approximately 0.5 mm between the ringlets. A schematic of the emissive probe design appears in Fig. 3 and a photograph of the emissive probe appears in Fig. 4. Unfortunately, at high discharge voltage the graphite paint could not withstand the harsh environment internal to a Hall thruster and for this reason, the graphite ringlets were not used for data presented below.

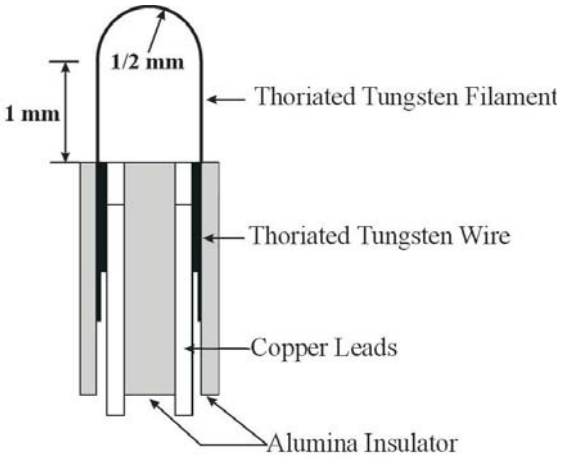

Figure 3. Emissive Probe Schematic

Even without the low secondary electron coating, the perturbations to the discharge current is below 15-20%. Oddly, the largest perturbation occurred at the lowest discharge voltage settings, which is inconsistent with the trends observed by other investigators.[13]

The diameter of the emitting filament is 0.0127 cm, which is much smaller than the electron gyroradius inside the Hall thruster. This condition is necessary for unmagnetized probe theory to be valid.[22,23] The filament size used in these measurements is of the same emitter diameter used by Haas[9] and similar to the emitter diameter used by PPPL.[11-14,21,24]

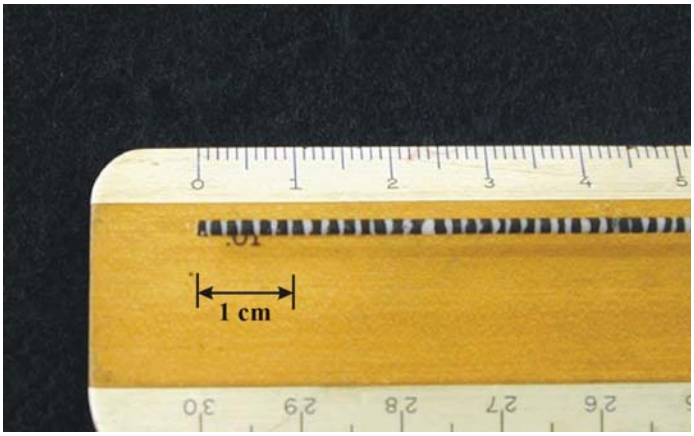

Figure 4. Emissive Probe Photograph

The area mapped by the emissive probes is displayed in Fig. 5. The origin is taken to be the location where the inner wall meets the anode. Five axial sweeps spaced 5 mm apart are taken inside the Hall thruster discharge channel. The probe is aligned so that the filament tip travels from 137 mm to within 10 mm of the anode. However, in order to accentuate the areas of interest, the results section only shows the emissive probe findings in the region from 0 to 100 mm. The emissive probe is positioned so that the plane of the filament loop is normal to the thruster radial direction. The expected resolution of the emissive probe is 1.5 mm, which is the approximate size of the filament loop. The probe residence time inside the discharge channel is kept below 80 ms.

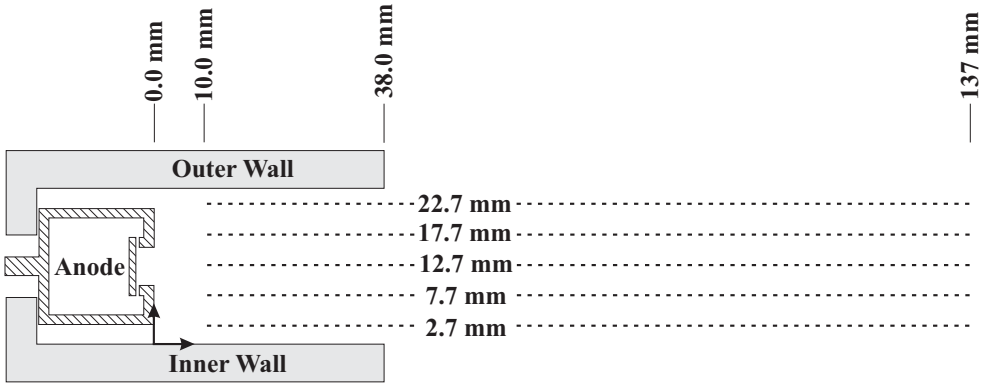

Figure 5. The Emissive Probe Mapping Region

The floating emissive probe circuit consists of the emissive probe, an isolation amplifier, and a floating power supply capable of supplying enough current to heat the filament. The floating emissive probe circuit is shown in Fig. 6. The sampling rate of the oscilloscope is dictated by the transit speed of the probe and is set to sample every 0.5 mm. This sampling speed is sufficient to easily capture the 1.5 mm resolution dictated by the probe dimensions. This sampling rate results in aliasing of the signal so that high frequency oscillations in the 10-30 kHz range, typical of the Hall thruster breathing mode, cannot be resolved. Therefore, the data presented constitute "time-averaged" measurements. The probe position and the perturbations to the discharge current and cathode potential are also recorded by the oscilloscope. During the post processing, a gentle spline smoothing[25] is used to reduce the signal noise from the probe position, and floating probe potential. Examples of a typical data sweep are given in Fig. 7, which shows the floating potential and the perturbations to the thruster as the probe is swept into the discharge channel. In this figure V_p is the plasma potential, V_k is the cathode potential and I_D is the discharge current.

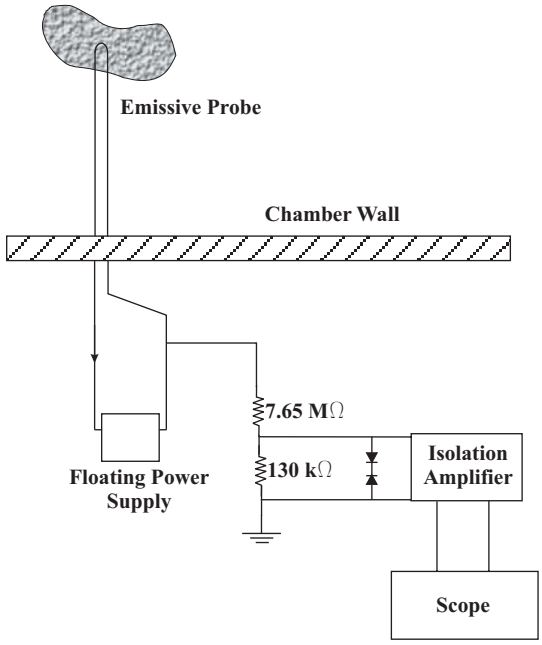

Figure 6. Floating Emissive Probe Circuit

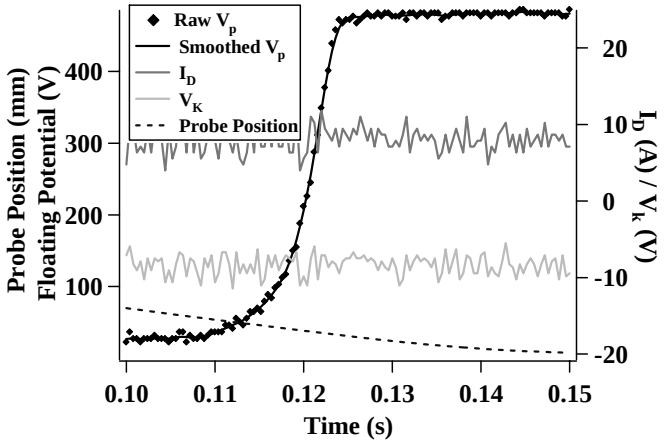

Figure 7. Emissive Probe Sweep Example

III. Data Analysis: Correction Method for the Space Charge Limited Sheath

A. Space Charge Limited Sheath

Space charge effects must be taken into account when analyzing emissive probe data in Hall thrusters. The space charge limit is reached when the emitted electron current to collected electron current ratio (δ) reaches a critical ratio (δ_c) that is approximately equal to one. Hobbs and Wesson[26] present an equation for critical emission given in Equ. 1, where m_e is electron mass and M_i is the ion mass.

$$\delta_c = 1 - 8.3\left(m_e / M_i\right)^{1/2} \tag{1}$$

As δ approaches δ_c, the electric field at the probe surface decreases and tends toward zero. Once δ becomes greater than δ_c, a potential well forms and emitted electrons are returned to the probe, creating a double sheath (solid line in Fig. 8). Three other lines are also shown in Fig. 8: i) $\delta < \delta_c$, insufficiency electron emission; ii) $\delta = \delta_c \approx 1$, space charge limited regime; and iii) $\delta >> 1$, strong electron emission.[27] Due to the extremely frailty of the emissive probe inside the harsh Hall thruster discharge channel environment, the heater current is increased slowly until adequate filament heating is reached. Adequate heating is reached when the plasma potential profile no longer changes with increased electron emission. This heating method ensures that the probe is operating in the space charge limited regime (regime ii).

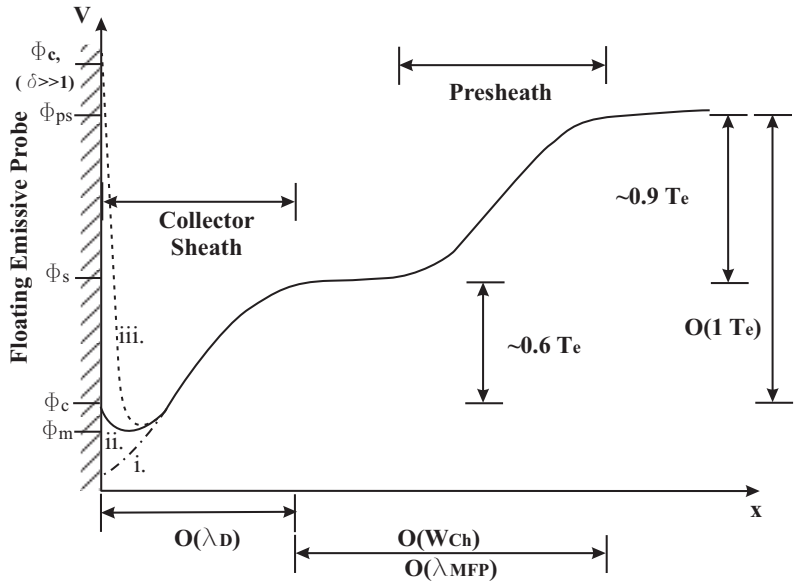

Figure 8. Emissive Probe Sheath. *The different operation regimes are shown by dashed lines and are labeled accordingly. (Not to scale)*

B. Collector Sheath

Adjacent to the emitting filament is the collector sheath. The potential drop across the collector sheath is important to the future discussion. The collector sheath region is on the order of a Debye length in size and has also been studied in great detail. Shwager[28] presents results that indicate the potential change in the collector sheath region to be 0.56 T_e for a D-T plasma with ion to electron temperature ratio of 0.1. Hobbs and Wesson[26] present equations for cold ions, which Schwager solves exactly. For large ion to electron mass ratios, Schwager found the potential drop across the collector sheath region to asymptote to less than 0.6 T_e. Even for very different temperature and ion species, there is still relatively good agreement between these two results. The value for the potential drop across the collector sheath region is taken to be 0.6 T_e.

C. Presheath

In addition to the collector sheath, there is a presheath separating the collector sheath and source plasma. A presheath forms in accordance to the Bohm criterion.[29,30] In order for a stable sheath to form, the ions at the quasineutral sheath edge must be accelerated to the Bohm velocity in the presheath region. It is also necessary for the electric field to be close to zero at the edge of the sheath. The dimension of the presheath is typically on the scale

of an ion mean free path (λ_{MFP}), which in our case is approximately as large at the Hall thruster discharge channel width (W_{ch}).[31] This fact presents difficulties that will be discussed later.

There has also been extensive work done to model the entire sheath (collector sheath and presheath) near a collecting and emitting wall. The total potential drop across the collector sheath and presheath is expected to be on the order of 1 T_e.[32] Schwager[28] suggests that the potential drop across the collector sheath and presheath should be approximately 1.5 T_e, a value that is commonly used by other researchers.[12-14,21,24] Stephens and Ordonez[33] offer an approximate expressions to estimate the collector sheath and presheath potentials. For xenon plasma with an ion to electron temperature ratio of 0.2 and with an emission ratio (δ) equal to δ_c, the potential drop from the source plasma to the collector is approximately 1.35 T_e. For the current analysis, 1.5 T_e will be used for the potential drop across the collector sheath and presheath.

D. Previous Correction Methods

Other experimenters[12,13,21] have augmented their floating emissive probe measurements by adding an electron temperature dependant correction term to the emissive probe measurements. This correction is used to account for the potential defect across the collector sheath and presheath in the space charge limited case. The technique uses 1.5 T_e for the plasma potential correction term.

This correction method creates a few challenges for the experimental results. Immediately upstream of the acceleration region, the electron temperature can be above 50 eV, which will result in a plasma potential correction of 75 V. This creates a large potential hump upstream of the acceleration region that is above the discharge voltage. This potential hump is not observed experimentally in this series of experiments. Additionally, internal to a Hall thruster, the entire region consists of large overlapping presheaths. With a highly non-uniform plasma and probe presheaths dimensions on the order of the discharge channel width,[31] it raises questions as to the most appropriate way to correct for the sheath potential defect. Also, the suggestion of 1.5 mm resolution for the emissive probe measurements is brought into greater question with the relatively huge presheaths.

There are several other complications to cloud the appropriate emissive probe correction. There are cases where the emissive probe will operate ideally ($\delta>\delta_c$) due to charge exchange (CEX) ions. When the CEX mean free path is on the same order as the plasma sheath potential structure, the slow moving ions fill the potential well and the sheath will not reach the space charge limit.[27,28] The CEX mean free path is approximately of 3 cm (assuming T_i~1 eV and n_n~5×10^{11} cm^{-3}). Keidar[31] suggests that the presheath is on the same order as the discharge channel (2.54 cm) whereas Intrator et al.[27] would suggest that total potential structure (collector sheath and presheath) is approximately 30-50 Debye lengths (0.3 cm). The effect of CEX ions on the space charge limited sheath is not clear, but the behavior is worth considering.

Aside from this, there are several other factors that complicate the space charge limited sheath. Aforementioned models assume large uniform plasma with a Maxwellian electron energy distribution that is far from the case inside the Hall thruster discharge channel. Most models assume a planer emitting surface, but the wire diameter is about equal to a Debye length, which places the probe between the thin sheath and OML regimes. The magnetic field also changes the electron dynamics near the probe. A slight probe misalignment can have a large effect on the probe collection area.

There is also the effect of strongly drifting plasma. The maximum emitted current and therefore the measured plasma potential is greatly increased due to the presence of positive ions that act to cancel the space charge. Particularly in drifting plasma, the collected ion current can be substantial. However, the regions of greatest concern, namely the regions of high electron temperature, are upstream of the acceleration zone and the effect due to drifting plasma is not important.

E. Correction Method

In summary, space charge limitations decrease the emitted electron current and results in floating potential measurement that is below the true plasma potential. While some sort of correction should be used to account for the effect, a simple correction is not possible due to overlapping potential structures from the channel walls and emissive probe and the lack of a robust model that can appropriately model the space charge limited sheath surrounding the emissive probe.

To account for the inaccuracies in the measurement, the following correction is suggested. The under predicted plasma potential is augmented by the collector sheath potential drop (0.6 T_e). This will give the instantaneous plasma potential local to the emissive probe. The collector sheath size (~O(λ_D)) internal to the Hall thruster is on the same order as the wire diameter, which is an order of magnitude smaller than the total emitting tip dimensions and therefore the desired resolution of approximately 1.5 mm is maintained. For reasons addressed previously, the effect from the probe presheath cannot be so simply addressed and should be considered a perturbation to the plasma. The

presheath potential drop should be used only to define error bars for the measurement. The corrected measurement will be correct to within ±0.9 T_e. In addition to the presheath perturbation, the one half of the potential drop across the floating heater power supply should also be included in the error. The heater filament potential drop is 4 V. The total error associated with the plasma potential measurements is equal to ±0.9 T_e-2V. It is important to point out that for any of the aforementioned plasma potential corrections the location and length of the acceleration zone will not be significantly changed.

Electron temperature can be calculated by using both "hot" and "cold" probe measurements. Equation 2 uses the potential drop across the total sheath to calculate the electron temperature. In this equation, k_B is the Boltzmann constant, T_e is the electron temperature, V_f is the cold probe floating potential, and e is the electron charge. The error in this temperature calculation is ±17%.[11]

$$V_p - V_f = -\frac{k_B T_e}{e} \ln\left(0.61\sqrt{\frac{2\pi m_e}{M_i}}\right) \tag{2}$$

Axial and radial electric fields at each location inside the thruster is also presented below. A central difference method is used with the plasma potential to calculate the electric field. The forward difference technique is used for the first point, and backward difference approach for the last point.

IV. Results and Discussion

The internal plasma potential structure is mapped for 4 operation points (See Table 1). Data are taken at discharge voltages of 300 and 500 V and 10 mg/s. For each operation point performance was optimized by monitoring thrust and thruster operating conditions to calculate real time efficiencies. The magnet settings are then varied until the *true* maximum efficiency for each operation point is found.

Table 1. Main Operation Points for Internal Plasma Potential Mapping

Point #	V_k (V)	V_d (V)	I_d (A)	Discharge Power (W)	M,Anode (mg/s)	M,Cath. (mg/s)	Current, IC (A)	Current, OC (A)	Current, TC (A)	Anode Effic. (%)
1	-10.5	300	9.17	2751	10.00	1.00	1.89	2.21	0.00	57.9
2	-10.9	300	8.95	2684	10.00	1.00	1.88	2.21	-0.51	61.2
3	-11.5	500	9.35	4675	10.00	1.00	2.90	2.67	0.00	61.6
4	-11.7	500	9.27	4635	10.00	1.00	2.90	2.87	-0.87	66.1

For each operating condition the corrected plasma potential, the electron temperature and axial electric field are given. For the 500 V cases, the radial electric fields are also given. From the plasma potential data, the start and end of the acceleration zone is determined by the location of 10 and 90% potential drop between the near anode and downstream region. The average start, end, and length of the acceleration region are given in Table 2. It can be seen in this table that the start of the acceleration zone is very similar for all but the 300 V, no trim coil case. The acceleration length may increase slightly with increased discharge voltage. The trim coil gives no conclusive trends as to the acceleration length and location. For all of the cases, a significant portion of the acceleration zone occurs outside of the discharge channel. It is likely that the location of the acceleration zone is dependent on axial variation of the electron mobility.[12,34] Although it is out of the scope of this paper, the electron mobility is an area for future study.

Table 2. Average Acceleration Region Boundaries

Point #	V_d (V)	Trim Coil?	Average Length (mm)	Average Start (mm)	Average End (mm)	% Outside Thruster
1	300	no	16.7	37.0	53.8	41.5
2	300	yes	15.8	32.3	48.1	26.5
3	500	no	17.2	32.2	49.4	30.0
4	500	yes	17.3	33.8	51.2	34.6

A. 300 V Cases

1. Haas's UM/AFRL P5 Mapping

Internal emissive results from Haas[9] for the UM/AFRL P5 Hall Thruster operation at 10 A and 300 V are shown in Fig. 9. Haas observed a strong defocusing of the equipotential lines. This behavior is observed by Haas is also computationally confirmed by Keidar[15]. Results from the internal emissive probe mapping of the NASA-173Mv1 at 300 V and 10 mg/s are shown below. Both the UM/AFRL P5 and the NASA-173Mv1 have the same discharge

channel dimensions. A comparison between these thrusters is important because it shows the effect that different magnetic field has on thrusters with similar discharge channel dimensions.

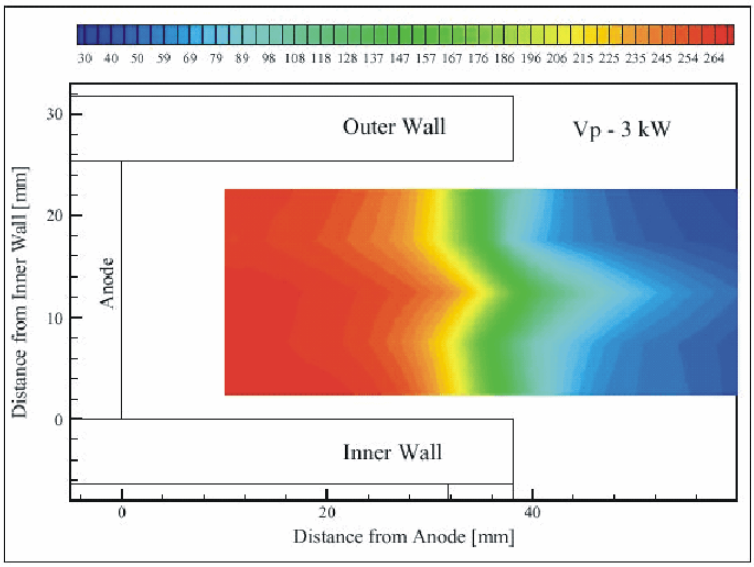

Figure 9. Internal Plasma Potential Map for the UM/AFRL P5 Hall Thruster operation at 10 A and 300 V

2. NASA-173Mv1 Mapping

The internal mapping for the 300 V xenon case without the trim coil is shown in Fig. 10 and the case with the trim coil is given in Fig. 11. The case without the trim coil shows a slight defocusing of the equipotential lines downstream of the acceleration region and a focusing in the main acceleration region. The slight asymmetry in the acceleration zone can be explained by the asymmetry in the magnetic field lines (not shown). The trim coil case shows slight equipotential focusing at both ends of the acceleration region. This result can be explained by the stronger plasma lens focusing and magnetic mirror effects of the trim coil. This behavior has also been predicted by Keidar[35] for a thruster using a magnetic mirror.

The location of maximum electron temperature begins just upstream and continues to the center of the acceleration zone for both the case with and without the trim coil. The maximum electron temperature is approximately 35 eV for the case without the trim coil. For the trim coil case, the electron temperature reaches a maximum of approximately 27 eV for most of the discharge channel although it does reach an electron temperature of 34 eV on the outer wall.

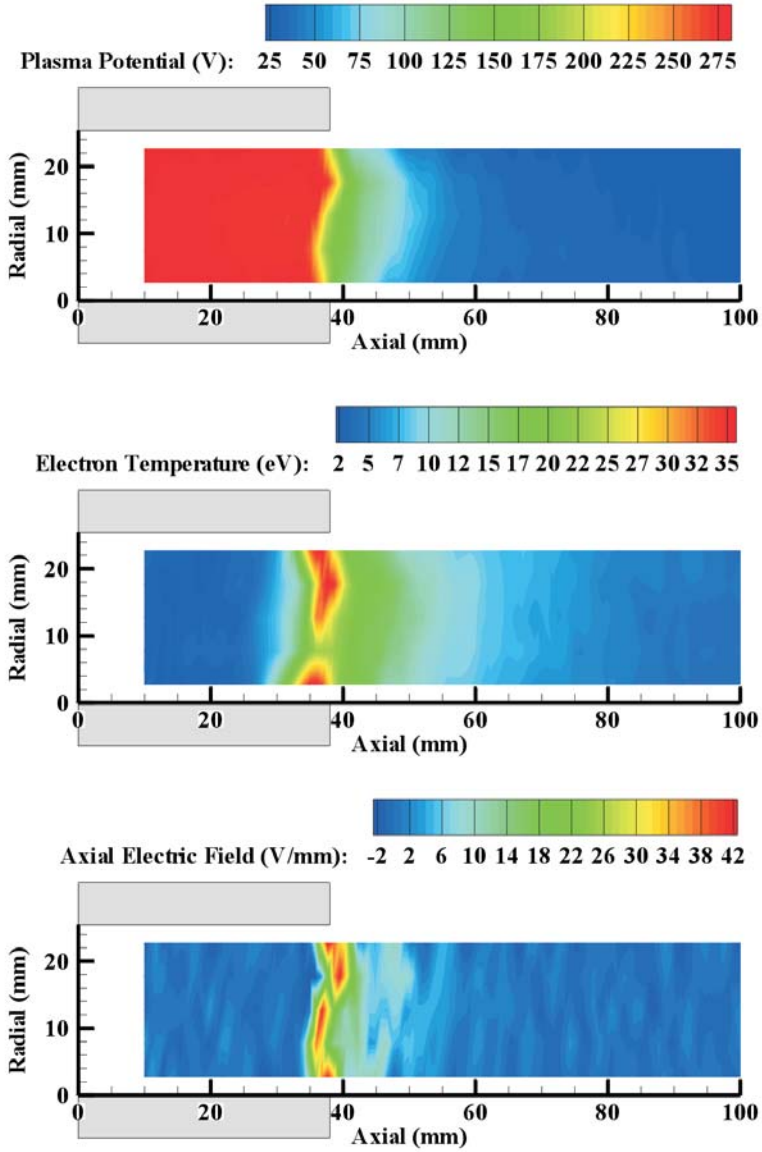

Figure 10. NASA-173Mv1 Internal Floating Emissive Probe Results for 300V Discharge Voltage, 102.4 sccm Anode Flow Rate, without the Trim Coil

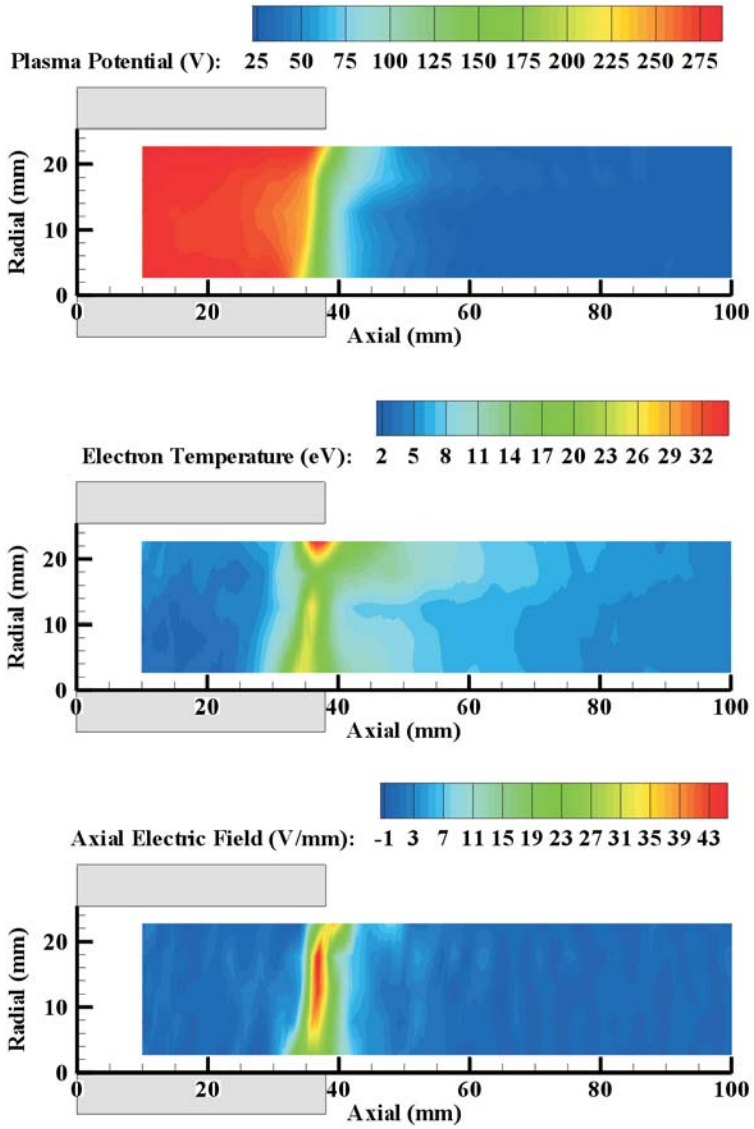

Figure 11. NASA-173Mv1 Internal Floating Emissive Probe Results for 300 V Discharge Voltage, 102.4 sccm Anode Flow Rate, with the Trim Coil

The acceleration region plots for the 300 V settings are given in Fig. 12. Although the finer details of the acceleration zone structure are lost on this plot, it is still possible to see the defocusing plasma potential structure in the non-trim coil case and the focusing plasma structure in the trim coil case. In this figure, it is shown that the large majority of the ion acceleration occurs outside of the discharge channel.

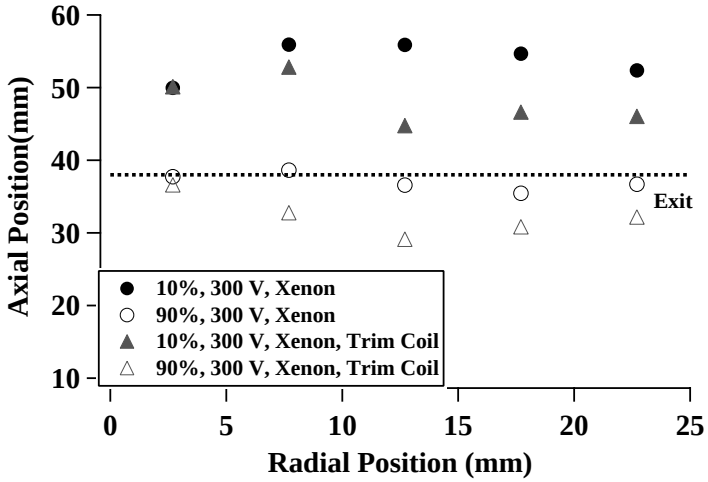

Figure 12. Acceleration Region Boundaries at 300 V Discharge Voltage and 102.4 sccm Anode Flow Rate

B. 500 V Cases

The internal emissive probe mapping for the 500 V at 102.4 sccm anode flow rate case without the trim coil is given in Fig. 14 and the trim coil case is given in Fig. 15. These cases show a remarkable correlation between the focusing magnetic field lines and the plasma potential. The non-trim coil case has an equipotential asymmetry that can be explained by an asymmetry in the magnetic field lines. The trim coil case has a strong focusing in the equipotential lines that is due to the strong focusing effect of the magnetic lens (Refer Fig. 2). Even the defocusing magnetic field lines downstream of the discharge channel correspond to defocusing equipotential lines. The radial electric field focusing the ions into the center of the discharge channel is approximately 12-18 V/mm while the axial electric field reached a maximum of about 70 V/mm in the trim coil case. For an unknown reason, the lens focusing effect is much more significant in the higher voltage conditions. The increased focusing at higher voltages is probably due to stronger magnetic fields, and the increased acceleration of ions. The higher voltage settings have greater ion acceleration, so any radial component is greater in magnitude and easier to measure experimentally.

Similar to the 300 V cases, both 500 V cases show a region of high electron temperature immediately upstream of the acceleration zone, which continues into the acceleration zone. The electron temperature of both trim coil and non-trim coil cases reaches a maximum of at 50 eV. As a result of increased Joule heating,[11,12,36,37] the electron temperature is higher for the 500 V cases then the 300 V cases. The higher voltage operation points also display an additional region of increased electron temperature near the anode, which is comparable to the "hot" region near the acceleration zone. The source of this anode heating is not clear, but this behavior is also observed by Meezan et al.[10] It could be the case that the emissive probe enters a different regime of operation that increased the error in the electron temperature calculation method. The existence of this near anode heating will be studied at a later date with single Langmuir probe measurements.

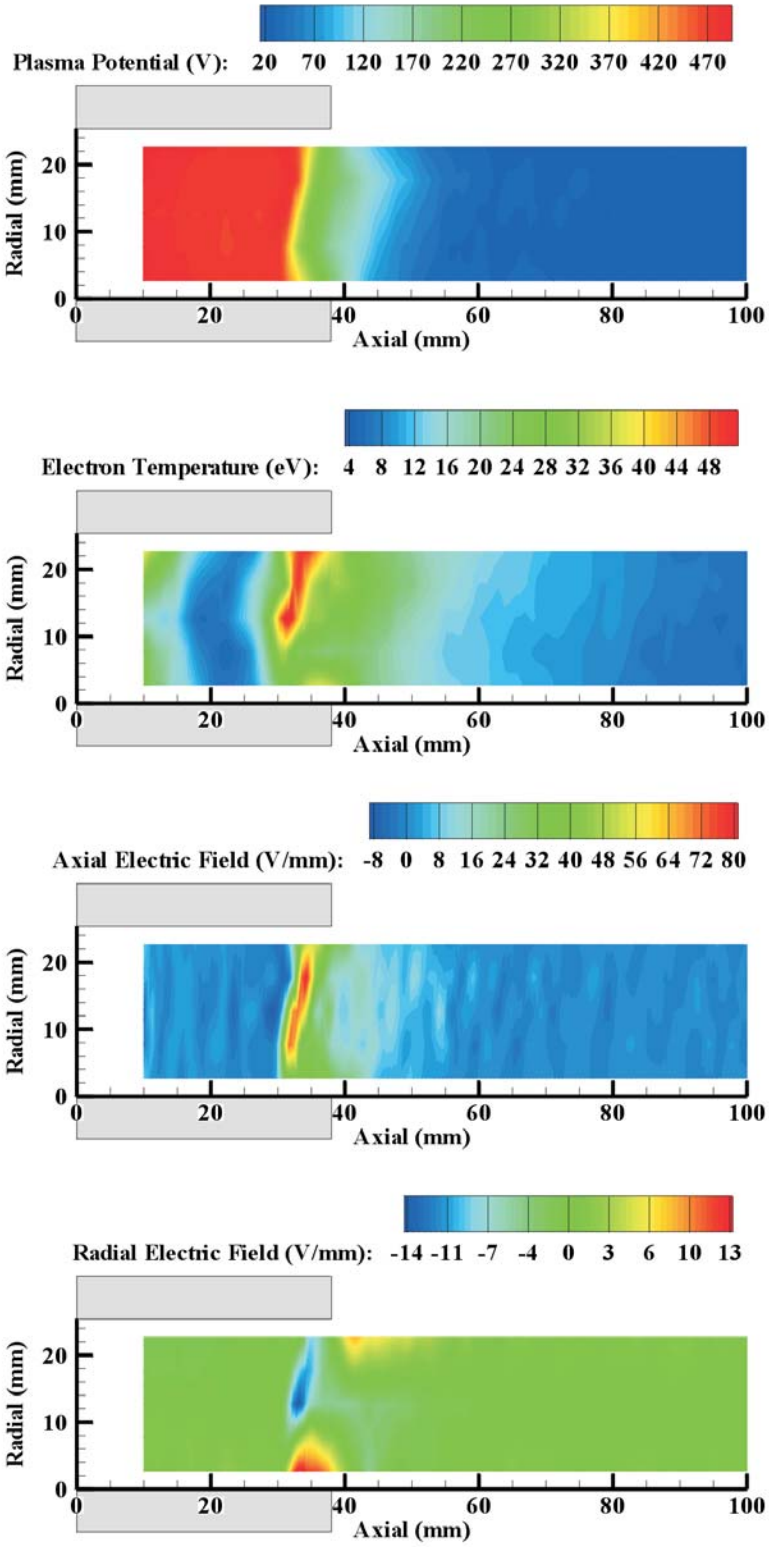

Figure 13. NASA-173Mv1 Internal Floating Emissive Probe Results for 500 V Discharge Voltage, 102.4 sccm Anode Flow Rate, without the Trim Coil

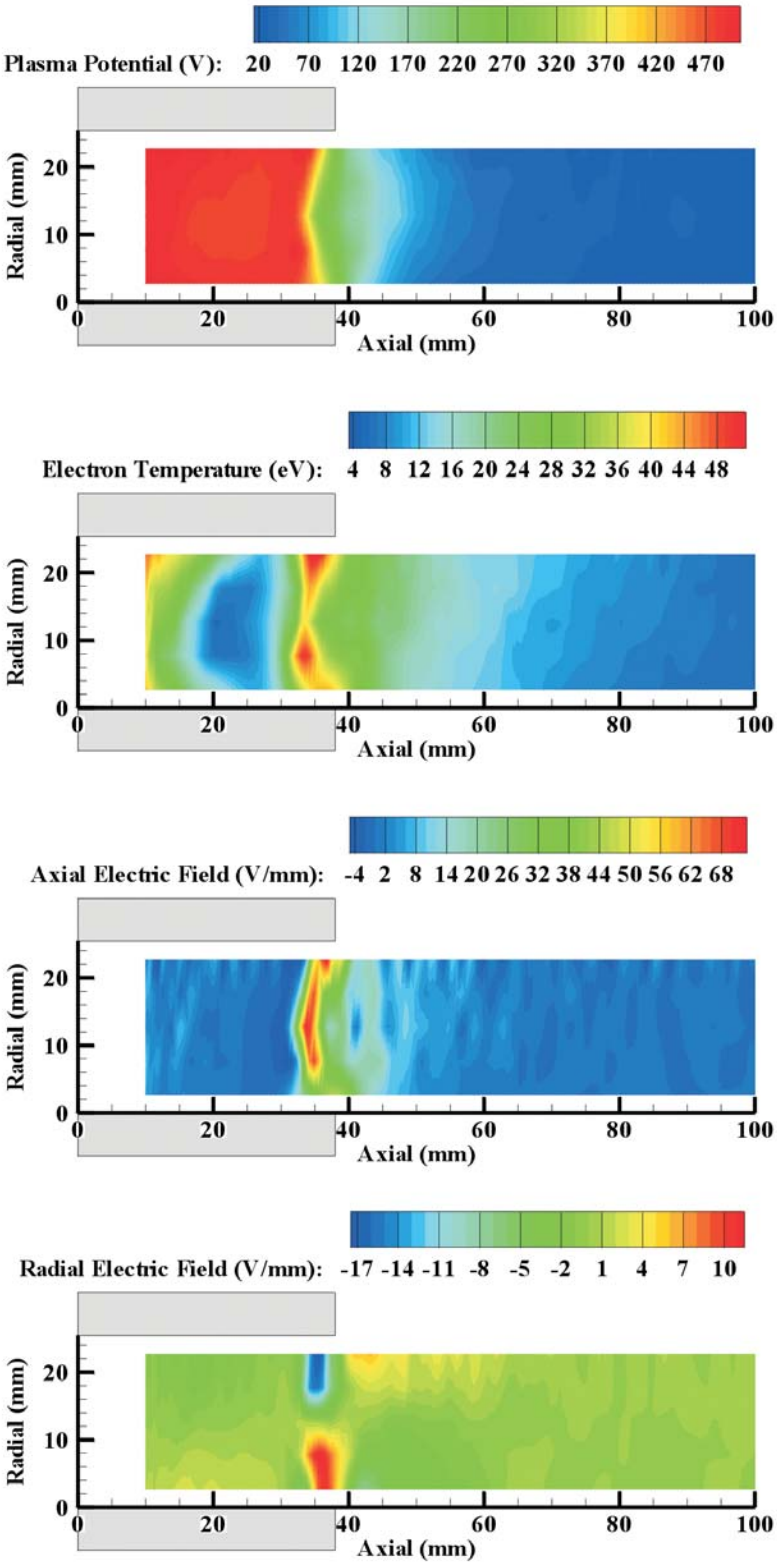

Figure 14. NASA-173Mv1 Internal Floating Emissive Probe Results for 500 V Discharge Voltage, 102.4 sccm Anode Flow Rate, with the Trim Coil

The acceleration zone for the 500 V case can be seen in Fig. 13. The figure displays the start and end of the acceleration zone. The length or location of the acceleration zone is not affected by the use of the trim coil.

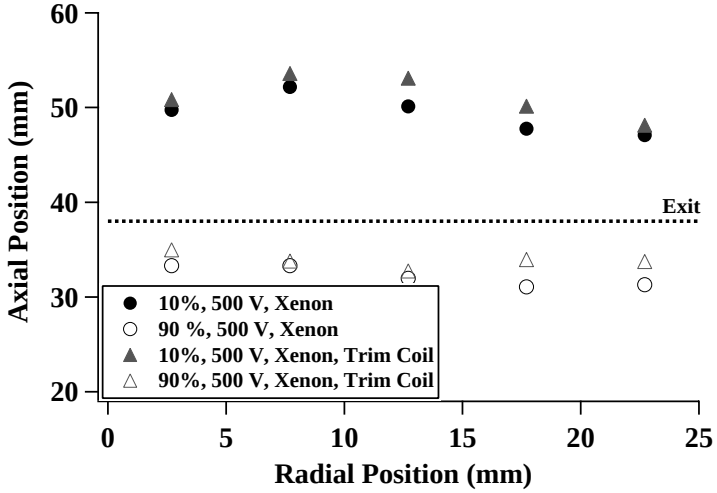

Figure 15. Acceleration Region Boundaries at 500 V Discharge Voltage and 102.4 sccm Anode Flow Rate

V. Conclusion

The internal plasma structure inside the NASA-173Mv1 has been successfully mapped. The plasma potential profile is shown to be strongly affected by the magnetic field topology. In the 500 V, trim coil case, the ions are shown to be strongly accelerated toward the center of the discharge channel. This effect has strong implications for future Hall thruster designs and Hall thruster life.

The trim coil is shown to strongly focus the ions toward the center of the discharge channel. Radial electric fields are often greater than 20% of maximum axial electric field. The magnetic field lines are shown to be closely related to the equipotential lines. This equipotential focusing is stronger with the high voltage cases. The trim coil may have a small effect on the acceleration zone location or length although more data is necessary before a conclusion can be made. The trim coil is found to have little effect on electron temperature. Maximum electron temperature increases with discharge voltage, and reaches approximately 35 and 50 eV for the 300 V and 500 V cases respectively.

Acknowledgments

We would like to thank the Association Francois-Xavier Bagnoud for their financial support during Mr. Jesse Linnell's graduate studies and NASA Glenn Research Center for financial support through research grant NCC04GA38G (grant monitor Mr. David Jacobson) and for the use of government equipment. Thanks also go to Dr. Michael Keidar and Dr. Yevgeny Raitses for their valuable discussion.

References

[1]Kim, V., "Main Physical Features and Processes Determining the Performance of Stationary Plasma Thrusters," Journal of Propulsion and Power, Vol. 14, No. 5, pp. 736-746, September-October 1998.

[2]Zhurin, V. V., Kaufman, H. R., Robinson, R. S., "Physics of Closed Drift Thrusters," Plasma Sources Science and Technology, Vol. 8, No. 1, pp. R1-R20, February 1999.

[3]Hofer, R. R., Gallimore, A. D., "The Role of Magnetic Field Topography in Improving the Performance of High-Voltage Hall Thrusters," *38th Joint Propulsion Conference*, Indianapolis, IN, July 7-10, 2002.

[4]Hofer, R. R., "Development and Characterization of High-Efficiency, High-Specific Impulse Xenon Hall Thrusters," Doctoral Thesis, Dept. of Aerospace Engineering, University of Michigan, Ann Arbor, MI, 2004.

[5]Linnell, J. A., Gallimore, A. D., "Efficiency Analysis of a Hall Thruster Operating with Krypton and Xenon," *41st AIAA/ASME/SAE/ASEE Joint Propulsion Conference*, Tucson, Arizona, July 10-13, 2005.

[6]Gavryshin, V. M., Kim, V., Kozlov, V. I., Maslennikov, N. A., "Physical and Technical Bases of the Modern SPT Development," *24th International Electric Propulsion Conference*, Moscow, Russia, Sept 19-23, 1995.

[7]Morozov, A. I., "Focusing of Cold Quasineutral Beams in Electromagnetic Fields," Soviet Physics - Doklady, Vol. 10, No. 8, pp. 775-777, February, 1966.

[8]Bugrova, A. I., Morozov, A. I., Popkov, G. B., Kharchevnikov, V. K., "Characteristics of a Plasma Lens," Soviet Physics. Technical Physics, Vol. 31, No. 2,
[9]Haas, J. M., Gallimore, A. D., "Internal Plasma Potential Profiles in a Laboratory-Model Hall Thruster," Physics of Plasmas, Vol. 8, No. 2, pp. 652-660, February 2001.
[10]Meezan, N. B., Hargus, W. A., Cappelli, M. A., "Anomalous Electron Mobility in a Coaxial Hall Discharge Plasma," Physical Review E, Vol. 63, No. 026410, January 24, 2001.
[11]Raitses, Y., Staack, D., Smirnov, A., Fisch, N. J., "Space Charge Saturation Sheath Regime in Hall Thrusters," Physics of Plasmas, May 2005.
[12]Raitses, Y., Staack, D., Keidar, M., Fisch, N. J., "Electron-Wall Interaction in Hall Thrusters," Physics of Plasmas, Vol. 12, No. 5, May 2005.
[13]Raitses, Y., Staack, D., Dorf, L., Fisch, N. J., "Experimental Study of Acceleration Region in a 2 kW Hall Thruster," *39th Joint Propulsion Conference*, Huntsville, Alabama,
[14]Staack, D., Raitses, Y., Fisch, N. J., "Temperature Gradient in Hall Thrusters," Applied Physics Letters, Vol. 84, No. 16, pp. 3028-3030, April 2004.
[15]Keidar, M., Gallimore, A. D., Raitses, Y., Boyd, I. D., "On the Potential Distribution in Hall Thrusters," Applied Physics Letters, Vol. 85, No. 13, pp. 2481-2483, 27 September 2004.
[16]Dushman, S., *Scientific Foundations of Vacuum Technique*, Vol. 4, Wiley, New York, 1958.
[17]Lide, D. R., *CRC Handbook of Chemistry and Physics*, 73rd Edition Ed., CRC Press, Boca Raton, Ann Arbor, London, Tokyo, 1992.
[18]Dymond, J. H., Smith, E. B., *The Virial Coefficients of Pure Gases and Mixtures, a Critical Compilation*, Oxford University Press, New York, 1980.
[19]Haas, J. M., "Low-perturbation Interrogation of the Internal and Near-field Plasma Structure of a Hall Thruster Using a High-Speed Probe Positioning System," Thesis, Dept. of Aerospace Engineering, University of Michigan, 2001.
[20]Haas, J. M., Gallimore, A. D., McFall, K., Spanjers, G., "Development of a High-Speed, Reciprocating Electrostatic Probe System for Hall Thruster Interrogation," Review of Scientific Instruments, Vol. 71, No. 11, pp. 4131-4138, November 2000.
[21]Staack, D., Raitses, Y., Fisch, N. J., "Sheilded Electrostatic Probe for Nonperturbing Plasma Measurements in Hall Thruster," Review of Scientific Instruments, Vol. 75, No. 2, pp. 393-399, February 2004.
[22]Kagan, Y. M., Perel, V. I., Soviet Physics - Technical Physics, Vol. 13, pp. 1348, 1969.
[23]Hershkowitz, N., Cho, M. H., "Measurement of Plasma Potential Using Collecting and Emitting Probes," Journal of Vacuum Science and Technology A, Vol. 6, No. 3, pp. 2054-2059, May/June 1988.
[24]Dorf, L., Raitses, Y., Fisch, N. J., "Electrostatic Probe Apparatus for Measurements in the Near-Anode Region of Hall Thrusters," Review of Scientific Instruments, Vol. 75, No. 5, pp. 1255-1260, May 2004.
[25]Reinsche, C. H., "Smoothing by Spline Functions," Numerische Mathematik, Vol. 10, pp. 177-183, 1967.
[26]Hobbs, G. D., Wesson, J. A., "Heat Flow Through a Langmuir Sheath in the Presence of Electron Emission," Plasma Physics, Vol. 9, pp. 85-87, 1967.
[27]Intrator, T., Cho, M. H., Wang, E. Y., Hershkowitz, N., Diebold, D., DeKock, J., "The Virtual Cathode as a Transient Double Sheath," Journal of Applied Physics, Vol. 64, No. 6, pp. 2927-2933, 1988.
[28]Schwager, L. A., "Effects of Secondary and Thermionic Electron Emission on the Collector and Source Sheaths of a Finite Ion Temperature Plasma Using Kinetic Theory and Numerical Simulation," Physics of Fluids B: Plasma Physics, Vol. 5, No. 2, pp. 631-645, 1993.
[29]Bohm, D., *The Characteristics of Electrical Discharges in Magnetic Field*, McGraw-Hill, New York, 1949.
[30]Riemann, K. U., "The Bohm Criterion and Sheath Formation," Journal of Physics D: Applied Physics, Vol. 24, pp. 493-518, December 1990.
[31]Keidar, M., Boyd, I. D., Beilis, I. I., "Plasma Flow in Plasma-Wall Transition in Hall Thruster Channel," Physics of Plasmas, Vol. 8, No. 12, pp. 5315-5322, December 2001.
[32]Chen, F. F., "Electric Probes," Plasma Diagnostic Techniques, R. H. Huddlestone and S. L. Leonard, eds., Academic Press, New York,1965.
[33]Stephens, K. F., Ordonez, C. A., "Sheath and Presheath Potentials for Anode, Cathode and Floating Plasma-Facing Surfaces," Journal of Applied Physics, Vol. 85, No. 5, pp. 2522-2527, 1 March 1999.
[34]Hagelaar, G. J. M., Bareilles, J., Garrigues, L., Boeuf, J.-P., "Role of Anomalous Electron Transport in a Stationary Plasma Thruster Simulation," Journal of Applied Physics, Vol. 93, No. 1, pp. 67-75, 15 October 2002.
[35]Keidar, M., Boyd, I. D., "On the Magnetic Mirror Effects in Hall Thrusters," Applied Physics Letters,
[36]Ahedo, E., Escobar, D., "Influence of Design and Operation Parameters on Hall Thruster Performances," Journal of Applied Physics, Vol. 96, No. 2, pp. 983-992, July 2004.
[37]Barral, S., Makowski, K., Peradzyski, Z., Gascon, N., Dudeck, M., "Wall Material Effects in Stationary Plasma Thrusters. II. Near-Wall and In-Wall Conductivity," Physics of Plasmas, Vol. 10, No. 10, pp. 4137-4152, October 2003.